Letter

Nonequilibrium Solvent Effects during Photodissociation in Liquids: Dynamical Energy Surfaces, Caging, and Chemical Identity

Andy Vong,*,# Devon R. Widmer,*,# and Benjamin J. Schwartz*
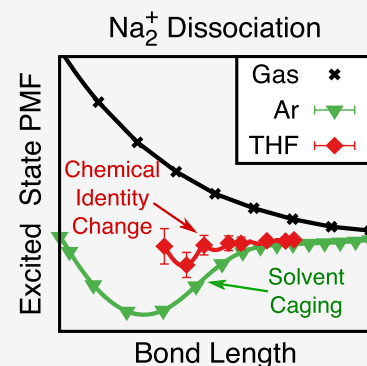
Read Online

ACCESS | 📊 Metrics & More | 📖 Article Recommendations | 🔲 Supporting Information

ABSTRACT: In the gas phase, potential energy surfaces can be used to provide insight into the details of photochemical reaction dynamics. In solution, however, it is unclear what potential energy surfaces, if any, can be used to describe even simple chemical reactions such as the photodissociation of a diatomic solute. In this paper, we use mixed quantum/classical (MQC) molecular dynamics (MD) to study the photodissociation of Na_2^+ in both liquid Ar and liquid tetrahydrofuran (THF). We examine both the gas-phase potential surfaces and potentials of mean force (PMF), which assume that the solvent remains at equilibrium with the solute throughout the photodissociation process and show that neither resemble a nonequilibrium dynamical energy surface that is generated by taking the time integral of work. For the photodissociation of Na_2^+ in liquid Ar, the dynamical energy surface shows clear signatures of solvent caging, and the degree of caging is directly related to the mass of the solvent atoms. For Na_2^+ in liquid THF, local specific interactions between the solute and solvent lead to changes in chemical identity that create a kinetic trap that effectively prevents the molecule from dissociating. The results show that nonequilibrium effects play an important role even in simple solution-phase reactions, requiring the use of dynamical energy surface to understand such chemical events.

Most chemical reactions, including photodissociation reactions that use light to break chemical bonds, take place in solution. Since solution-phase reactions are inherently more complex than those in the gas phase, most studies of photodissociation and recombination dynamics have focused on simple diatomic molecules to elucidate solvent effects on chemical reaction dynamics,[1−7] with a particular emphasis on molecular iodine (I_2).[8−13]

How can one use energy surfaces to think about solute and solvent motions involved in solution-phase photodissociation? For the solute, a common approach when considering solution-phase reactions is to simply assume that the solute moves on the same potential energy surfaces as in the gas phase.[1] We have shown in recent work, however, that the Pauli repulsion interactions between the solvent and the solute's bonding electrons can change the electronic structure of diatomic solutes, inducing large instantaneous dipole moments and causing changes in the vibrational frequency and dissociation energy.[14] Moreover, we also have found that when there are local specific interactions between the solvent molecules and the solute that only need to have a strength comparable to that of a hydrogen bond, the electronic structure and even the chemical identity of the solute can be dramatically altered.[15,16] Thus, one needs to go beyond gas-phase surfaces and include the way in which solutes and solvents interact to understand solution-phase chemical reactions.

Rather than assuming the solute moves on the same potential energy surface as in the gas phase, the solute could be thought of as moving along an effective potential energy surface where the solvent is at equilibrium with the solute, the so-called potential of mean force (PMF).[17] Such an approach can describe, on average, how the solvent will interact with and potentially alter the electronic structure of the solute, presuming that the solvent truly does remain in equilibrium throughout the course of the reaction.[1,5,6] For example, PMFs are appropriate for thinking about ion pairs in liquid water: solute−solvent structures identified in the ground-state PMF[18,19] have been associated with those found with X-ray absorption,[20] neutron scattering,[21] and Raman spectroscopy.[22] And several groups have used PMFs to understand how solvent effects can alter electronic structure during proton transfer,[23] electron transfer,[24] proton-coupled electron transfer,[25] hydride transfer,[26] etc. and following electronic excitation of a dye molecule used as a solvation probe.[27]

For all of the success of using PMFs to interpret solution-phase chemistry, one generally does not expect the assumption of the solvent remaining at equilibrium to hold for a molecularly violent event like photodissociation, or even for chemistry that takes place on electronic excited states. Ishida and Rossky[27,28] used excited-state PMFs to understand the solvent reorganiza-

tion following the photoexcitation of a betaine dye. There also have been a few studies that used a semiempirical description to concoct the potential energy surfaces governing solute motion following photoexcitation in solution.[7,29] However, we are not aware of any investigations exploring the quantum mechanics of how solvents alter the electronic structure and excited-state reaction dynamics of molecules in liquids, and for photodissociation in particular, one would not expect an equilibrium description to properly account for the strong "caging" solvent collisions that promote recombination.[5] Thus, one of the primary goals of this work is to explore the use of a rigorous formalism, based on the time integral of work,[30] to describe nonequilibrium photodissociation dynamics in solution.

The key questions explored in this paper are, what type of potential energy surfaces should be used to think about the dynamics during condensed-phase photodissociation reactions? Given that the dissociation pathway can depend on solvent effects like caging or complexation, is it appropriate to think of the solvent as being in equilibrium with the solute, and if not, why not? If equilibrium energy surfaces do not capture solute and/or solvent dynamics, how should one think about the nonequilibrium dynamics? And what generalities about solution-phase photodissociation reactions can be learned by studying model systems, especially when local specific solute–solvent interactions can potentially alter the chemical identity of the solute?[15,16]

In this Letter, we directly address all of these questions through mixed quantum/classical (MQC) molecular dynamics (MD) simulations of Na_2^+ in both liquid Ar and liquid tetrahydrofuran (THF). We choose this system because we already have explored how solvent interactions alter the ground-state solute electronic structure for both Na_2[14,15] and Na_2^+[16] in these solvents; we focus on Na_2^+ here because it dissociates (in the gas phase) when placed on its lowest electronic excited state[31] and Na_2 does not. We find that taking the time integral of work leads to a dynamical energy surface that captures key solvent effects for understanding photodissociation of Na_2^+ in both Ar and in THF. In particular, solvent caging dominates the photodissociation dynamics of Na_2^+ in liquid Ar, something that is well-captured by the dynamical energy surface but not properly accounted for by the gas-phase surfaces or PMFs. For the photodissociation dynamics of Na_2^+ in THF, the dynamical energy surface shows how local specific interactions that dynamically change the solute's chemical identity create a kinetic trap that effectively prevents the molecule from dissociating the way it would at equilibrium.

To investigate the type of potential energy surfaces that best elucidate the dynamics of condensed-phase photodissociation, we performed a series of MQC MD simulations, the computational specifics of which are summarized in the methods section below and detailed in the Supporting Information. Briefly, we treat the Na_2^+ molecule as two classical Na^+ cores that are held together by a single quantum mechanical valence bonding electron. We utilize previously developed pseudopotentials[32] to describe the interaction between the bonding electron and the Na^+ cores[33] and 254 THF molecules[34−36] or 1600 Ar[37] atoms and solve the Schrodinger equation for the electron in a basis of 32^3 grid points in Ar and 64^3 grid points in THF. This methodology reproduces gas-phase quantum chemistry calculations quite well[31,33] and also has successfully reproduced the experimental properties of sodium cation:solvated electron tight-contact pairs in THF.[36,38] Here, we calculate the behavior of the Na_2^+ molecule in 120 K liquid Ar at a density of 1.26 g/

mL, well in the liquid region of the phase diagram, and at 298 K in liquid THF at the experimental density at 1 atm of 0.89 g/mL.

First, we generated PMFs where the solvent in is equilibrium with the solute by holding the Na—Na bond length at fixed distances through the application of an umbrella potential[39] centered at the bond distance of interest; we let the condensed-phase system equilibrate at each distance and then calculated the average energy while running the system on both the ground and first excited electronic states. Stitching together these energies as a function of distance using the MBAR method[40] produced PMFs, which are shown in Figure 1, where the solvent is in
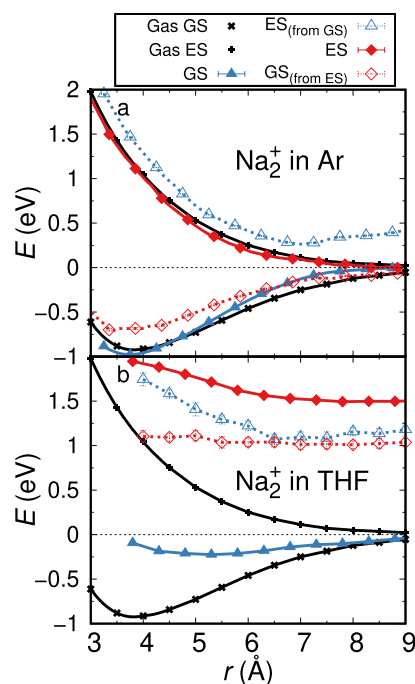

Figure 1. Potentials of mean force for the Na_2^+ molecule in Ar and $Na_2(THF)_n^+$ in THF are shown. The Na_2^+ gas-phase potential energy surfaces are plotted as the black curves. The condensed-phase PMFs are plotted as solid blue triangles for the ground state, solid red diamonds for the excited state, dashed blue curves for the excited state calculated while propagating the solvent dynamics on the ground state, and dashed red curves for the ground state calculated while propagating the solvent dynamics on the excited state. Panel a shows the PMFs for Na_2^+ in Ar while panel b shows the results in THF. A comparison of the solid and dashed curves shows that the solvent structures are different for the ground and excited electronic states so that the PMF for the excited state cannot be generated from studying equilibrium configurations on the ground state.

equilibrium with the solute. One question is whether the excited-state PMF can be generated while the solvent is in equilibrium with the solute's ground state and vice versa. In other words, are the solvent structures and fluctuations associated with the two solute electronic states similar enough that the PMFs are independent of which electronic state we choose?

The black curves in Figure 1 show the ground- and first excited-state potential energy surfaces of the Na_2^+ molecule in the gas phase calculated with our MQC methodology; the curves do an excellent job reproducing the known potential energy surfaces of this molecule, including the ground-state vibrational frequency, bond dissociation energy, and the lowest-energy electronic absorption.[31] The solid, colored curves in Figure 1

show the ground- (blue solid triangles) and first excited-state (red solid diamonds) PMFs for Na_2^+ in Ar (panel a) and in THF (panel b) calculated with the solvent at equilibrium with the solute occupying the electronic state under investigation. The data in Figure 1a show that on the Na_2^+ electronic ground state, compared to the gas phase, interactions with liquid Ar lead to a shorter equilibrium bond length (3.74 Å in Ar vs 3.84 Å in the gas phase) and a higher Na—Na vibrational frequency (134 cm^{-1} in Ar vs 113 cm^{-1} in the gas phase), much like we observed previously for the Na_2 molecule.[14-16] The red solid diamonds show that when the molecule is placed on the electronic excited state, the PMF is nearly identical to the potential energy surface in the gas phase, indicating that the equilibrium excited-state solvent interactions are small compared to the intrinsic gas-phase energy.

The dashed, colored curves in Figure 1a test whether PMFs for one solute electronic state can be predicted when the solute resides in a different electronic state. The blue open triangles show the Na_2^+ first excited state while the solvent is equilibrated with the electronic ground state; this prediction yields a dissociative surface that is raised in energy relative to the gas phase because when the solvent is equilibrated around the ground-state solute, it is in an unfavorable geometry for solvating the solute excited state. The red open diamonds show that when the solvent is equilibrated for the solute's excited state, there is a significant desolvation and thus an increase in energy and decreased vibrational frequency of the ground electronic state. Thus, as might be expected, we cannot accurately predict the excited-state PMF while the solute resides in its electronic ground state because the way the solvent equilibrates around one solute electronic state destabilizes the other electronic state.

Although the PMFs for Na_2^+ in Ar are qualitatively similar to the gas-phase potentials, the situation turns out to be completely different for Na_2^+ in liquid THF. In previous work, we found that the oxygen atoms on THF make weak dative bonds with the Na^+ cores inside the Na_2^+ molecule.[15,16] These dative bond interactions are only about the same strength as a hydrogen bond (~4 kcal/mol), but they cause the bonding electron density to be pushed out of the internuclear region, leading to a significant increase in bond length (the bond length changes from 3.84 Å in the gas phase to 5.24 Å in liquid THF) and a factor of ~3 decrease in both vibrational frequency (from 113 to 42 cm^{-1}) and bond dissociation energy (from 0.92 eV in the gas phase to 0.23 eV in THF).[16] We also found that the dative bonding interactions stabilize the Na_2^+ solute in two primary coordination states: $Na(THF)_4-Na(THF)_5^+$ and $Na(THF)_5-Na(THF)_5^+$. These coordination states behave as distinct molecules whose chemical identities are different both from gas-phase Na_2^+ and from each other; the two coordination states are in equilibrium with each other and have to surmount a barrier of ~8 k_BT to interconvert.[16] Each coordination state has its own bond length, vibrational frequency, and dissociation energy. In other words, in THF, the solvent has integrated itself as part of the chemical identity of two different Na_2^+-based solutes.[15]

Figure 1b shows that because of the change in chemical identity from Na_2^+ to Na_2^+:$(THF)_n$, the PMFs for the Na_2^+ molecule in THF are entirely different from those in the gas phase or in liquid Ar. Furthermore, comparison of the solid and dashed curves show that the ground- and excited-state solvent structures are dramatically different from one another. Surprisingly, the most prominent feature in Figure 1b is that unlike in the gas phase or liquid Ar, the excited-state PMF for

Na_2^+ solvation on the excited state (solid red diamonds) in THF is hardly dissociative.

To test the ability of PMFs in predicting photodissociation dynamics, we used the time integral of work formalism[30] to describe the actual potential energy surface followed during the adiabatic nonequilibrium dynamics. We ran a series of nonequilibrium trajectories, 15 in Ar and 20 in THF, starting from equilibrated configurations near the PMF minimum in the Na_2^+ electronic ground state (~3.7 Å in Ar; ~5.4 Å in THF) and then placed the molecule onto the electronic excited state to simulate photoexcitation. We then calculated the effective potential surface on which the excited Na_2^+ moved during nonequilibrium dissociation by

$$U(t) = -\int_{t_0}^{t} F(t)\, v(t)\, dt \tag{1}$$

where $F(t)$ is the total force (from the solute and solvent) on the Na nuclei along the bond axis, $v(t)$ is the bond velocity, and t_0 is the time at which photoexcitation takes place. Since we know the trajectory that the dissociating molecule takes, $r(t)$, we can parametrically combine $U(t)$ and $r(t)$ to produce an effective energy surface followed during the dynamics, $U(r)$, as described in the Supporting Information. The time t in eq 1 is chosen to range up to ~300 fs in liquid Ar and to ~1000 fs in liquid THF, which is long enough to have sampled all the appropriate photodissociation dynamics but short enough to avoid diffusive recrossings that occur at longer times.

In this paper, we refer to the nonequilibrium $U(r)$ as a "dynamical energy surface"; by construction, this energy surface incorporates the actual nonequilibrium dynamics followed during the chemical reaction without any assumptions regarding the gas-phase potential energy surfaces or maintaining equilibrium with the solvent. Our use of a dynamical energy surface in this instance was inspired by the work of Zanuttini et al., who studied the connection of solvent collisions to photodissociation pathways.[5] The nonequilibrium ensemble-averaged dynamical energy surface following photoexcitation of Na_2^+ in both liquid Ar and liquid THF are shown as the green curves in Figure 2. The raw trajectory data used to calculate the dynamical energy surfaces are shown in the Supporting Information for reference.

Figure 2a shows that following the initial excitation, the dynamical energy surface for Na_2^+ in liquid Ar has a slope that is quite similar to that in the gas phase, which is also very similar to the PMF. This is in agreement with prior work studying diatomic photodissociation in rare-gas solids.[5,13,41] But after the first ~1 Å (~60 fs) of separation, the dynamical energy surface in liquid Ar shows a positive slope; this occurs at exactly the internuclear distance at which the expanding Na_2^+ molecule collides with the first-shell solvent atoms; in the nonequilibrium dynamics, there is always a collision with the first solvent shell that exerts a force on the expanding molecule back toward shorter bond distances. By ~7 Å (~200 fs), the slope of the dynamical energy surface has decreased to roughly zero, indicating that the dissociated solute has on average escaped the solvent cage and that the dynamics are now governed more by diffusion than the electronic structure of Na_2^+. Clearly, neither the gas-phase surfaces nor the PMFs capture the dissociation dynamics of Na_2^+ in Ar because they do not capture solvent caging, which is by necessity a nonequilibrium effect: there are no strong directional collisions like this at equilibrium.

The green curve in Figure 2b shows the dynamical energy surface following photoexcitation of Na_2^+ in liquid THF. The
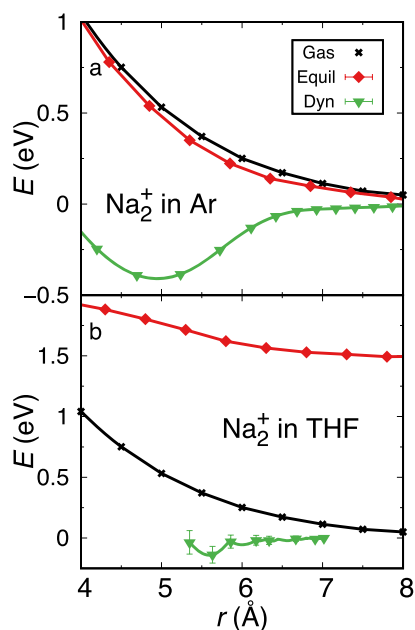
Figure 2. Dynamical energy surfaces reveal the shortcomings of gas-phase surfaces and equilibrium-based potentials of mean force for the photodissociation of Na_2^+ in solution. The potential energy surface for the first excited state of gas-phase Na_2^+ (black crosses) and the PMF for the electronic excited state (red diamonds) are the same curves as in Figure 1; the dynamical energy surface calculated from nonequilibrium trajectories parametrically with $r(t)$ using eq 1 (green triangles) is shown for Na_2^+ in Ar (panel a) and in THF (panel b). The dynamical energy surfaces show clear solvent-induced nonequilibrium features of the Na_2^+ dissociation reaction. In Ar, the well at ~5 Å in the dynamical energy surface is the result of nonequilibrium caging by the surrounding solvent, as explored further in Figure 3, below, while the gradual upward slope of the dynamical energy surface in THF comes from changes in the electronic structure and chemical identity of Na_2^+ in this solvent, as detailed in Figures 4 and 5, below.

dynamical energy surface displays two main features: a small initial "dip" at an internuclear separation of ~5.6 Å, followed by a slight increase in energy at longer distances. What this dynamical energy surface shows is that, following photoexcitation, the Na_2^+ species elongates but does not dissociate; the details of what causes this will be discussed below. The nonequilibrium dynamical energy surface shows a strong contrast to both the gas-phase (black curve) potential surface and the excited-state PMF (red diamonds), both of which predict that the molecule should dissociate.

To understand why gas-phase surfaces and PMFs fail in such different fashions for the photodissociation of Na_2^+ in liquid Ar and liquid THF, we next turn to exploring the nonequilibrium behavior in each solvent in more detail. In liquid Ar, the dissociation dynamics involves a strong interaction of the photofragments with the Ar solvent cage that does not occur at equilibrium. This leads to the question of whether an equilibrium approach could ever capture this type of caging event. To explore this, we tuned the time scale of the Ar solvent fluctuations by artificially changing the Ar mass while leaving all the intermolecular potentials unchanged; this means that the equilibrium solvation structures do not change, but the time scale for equilibration does. We then ran nonequilibrium trajectories with the altered solvent mass. Figure 3 shows that when the mass of the Ar atoms is reduced by a factor of 20 (purple squares) such that the Ar atoms are an order of
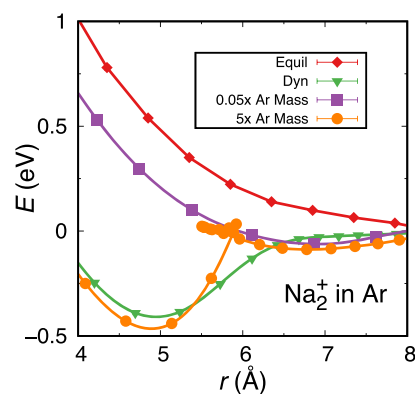

Figure 3. Dynamical energy surfaces from nonequilibrium simulations (computed via eq 1 parametrically with $r(t)$; see the Supporting Information) of the photodissociation of Na_2^+ in liquid Ar as a function of the Ar mass reveal that the magnitude of solvent caging is dependent on the time scale of the solvent fluctuations. When the Ar mass is divided by 20 (purple squares) and increased by a factor of 5 (orange circles) but the intermolecular potentials are left unchanged from the original simulations (green triangles, same curve as in Figure 2a), there are significant changes in the dynamical energy surface. For comparison, the excited-state PMF is shown as the red diamonds (same curve as in Figure 1a). When the solvent mass is reduced to the point where fluctuations occur on a time scale comparable to the Na_2^+ photodissociation dynamics, the dynamical energy surface begins to resemble the PMF. When the solvent mass is increased, however, the initial collision with the solvent cage knocks the photofragments back with much greater force, dynamics that are not seen at equilibrium. This leads to a temporary shortening of the Na−Na bond length before the fragments ultimately escape the solvent, creating the loop in the dynamical energy surface near 5.8 Å.

magnitude lighter than the Na^+ cores, the dynamical energy surface now strongly resembles the PMF (red diamonds). The solvent in this case is so light that the dissociating Na_2^+ molecule can easily push the nearby atoms aside, removing the "caging" event that dominated the dynamics when the Ar had its full mass. In other words, the artificially lighter Ar solvent can equilibrate on a time scale comparable to the time it takes photoexcited Na_2^+ to dissociate, so that an equilibrium approach predicts the nonequilibrium dynamics reasonably well.

Figure 3 also explores the other extreme, where the mass of the Ar solvent atoms is increased by a factor of 5 (orange curve) such that the Ar atoms are 10 times heavier than the Na^+ cores. Now the "cage effect" is exaggerated, as the dynamical energy surface shows not only a stronger reflection, but actually a small loop at internuclear separations near 5.8 Å, the result of the fact that the dissociating Na_2^+ solute has to undergo multiple bounces before being able to escape the surrounding solvent cage, as seen experimentally for I_2 in solid rare gas matrices.[11] Thus, even in a simple, noninteracting solvent like liquid Ar, an equilibrium picture will fail to describe photodissociation reactions when the time scale of dissociation is faster than the intrinsic time scale of the solvent fluctuations.

To better visualize the solvent caging in this system, Figure 4 shows plots of the average solvent positions around Na_2^+ in liquid Ar as a function of Na−Na distance both at equilibrium, panel a, and during the nonequilibrium photodissociation dynamics, panel b. The plots show an isosurface at solvent distances at about the van der Waals size of the solute molecule, ~3.3 Å from each Na^+ nucleus; the color represents the cylindrically averaged probability of finding a solvent atom at that point on the surface relative to the bulk solvent density. The
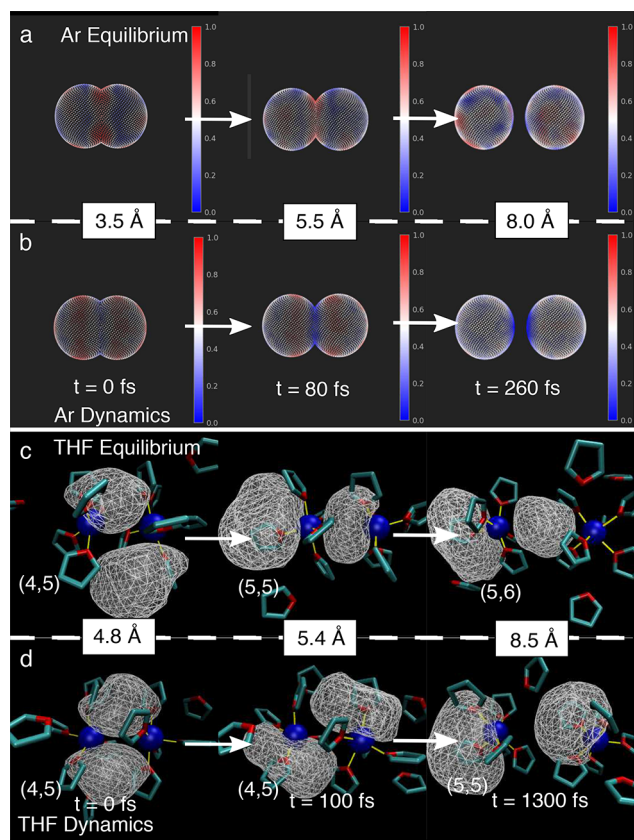
Figure 4. Representative solvent distributions around excited-state Na_2^+ at equilibrium, panel a, and during nonequilibrium dynamics, panel b, in liquid Ar are shown. The surfaces are ~3.3 Å from the Na^+ cores and colored to show the relative solvent density at that distance (bulk, white; red, excess; blue, deficit). During nonequilibrium dynamics, there is a larger chance of finding axial Ar and a smaller chance of finding equatorial Ar than at equilibrium, providing a direct visualization of caging. Corresponding representative snapshots of excited-state $Na(THF)_4$−$Na(THF)_5^+$ in liquid THF are shown at equilibrium, panel c, and during the nonequilibrium dynamics, panel d. Na^+ cores are plotted as blue spheres and THF as turquoise sticks with red O atoms. The bonding electron is drawn as a wire mesh containing 75% of the charge density. Following photoexcitation, the bonding electron density has its node oriented along the bond axis; however, rotation of the node (cf. Figure 5b, below) occurs differently at equilibrium (panel c) than following photoexcitation (panel d). The coordination of the Na_2^+ species by THF also changes differently at equilibrium and during the nonequilibrium dynamics (cf. Figure 5a).

red color indicates that more Ar is present than the average density, white color shows about an average amount of solvent, while blue color shows a deficit of solvent at that position. The points are evenly spaced so that the color density provides an accurate representation of the spatial density of solvent atoms.

The left-most plots compare the solvent distribution around Na_2^+ in Ar at equilibrium on the excited state (panel a) and at equilibrium on the ground state (panel b, which has a ground-state solvent configuration because it shows the Franck−Condon excited solute before the solvent has had time to move). Clearly, the equilibrium ground- and excited-state solvation structures are different. When the Na−Na bond is separated by 3.5 and 5.5 Å at equilibrium on the excited state (left and center plot in panel a), there is a clear preference for the solvent to reside near the "neck" of the molecule, as the excited-state electron density has a node between the two atoms, causing the

solvent to move into this region to maximize ion-induced dipole interactions. During the nonequilibrium dynamics, however, the center plot of panel b shows that there is a deficit of solvent in the neck region and an excess of solvent at the ends of the molecule as it encounters the solvent cage. The solvent has not had time during the ~80 fs since excitation to move into the neck region or away from the ends of the dissociating molecule, showing that caging is what causes the positive slope in this region of the dynamical energy surface. The memory of photoexcitation persists even as the molecule separates to 8 Å, which is 260 fs after excitation, as evidenced by the deficit of solvent on the inside of the bond in the right plot of panel b compared to the excited-state equilibrium prediction in panel a.

Unlike in liquid Ar, where the dynamical energy surface approaches the PMF and the gas-phase potential energy curve when the solvent fluctuates on fast time scales compared to the molecular dissociation, the dynamical energy surface for the photodissociation of Na_2^+ in liquid THF looks completely different because the chemical identity of the Na_2^+ molecule is intricately linked with its local solvent environment, such that the solute is better thought of as two different Na_2^+:$(THF)_n$ complexes.[15,16] To understand how the complexation by the solvent affects dissociation, we turn to Figure 4c,d (left), which shows that when Na_2^+:$(THF)_n$ is initially photoexcited to its lowest energy excited state, the node in the electron density lies oriented along the bond axis: the electronic structure resembles that of a molecular π bonding orbital rather than the σ^* antibonding orbital seen with gas-phase Na_2^+ or Na_2^+ in liquid Ar (see Supporting Information).[16] This is a reflection of the fact that the coordination complex in liquid THF is truly a different molecule with a chemical identity different from that of the gas-phase Na_2^+ species, leading to a very different electronic structure.

If we start from a $Na(THF)_4$−$Na(THF)_5^+$ configuration, as in Figure 4, the solute begins its dissociation process from its equilibrium ground-state distance of ~4.8 Å.[16] Following photoexcitation, the solute's Na−Na bond distance increases to ~5.4 Å after approximately 100 fs, but the electronic structure at this time (Figure 4d, center) is clearly very different from the equilibrium structure at the same distance (Figure 4c, center). The equilibrium picture when the bond length reaches this distance has the node of the electronic wave function perpendicular to the bond, creating a dissociative force. But the node in the wave function during the nonequilibrium dynamics is not able to fully rotate from parallel (in the Franck−Condon region) to perpendicular to the Na−Na bond. The rotation of the excited-state node requires significant rearrangement of the datively bonded THF molecules; there is simply insufficient time following excitation for these THFs to have reached their equilibrium stable orientation. Finally, even 1.3 ps after photoexcitation, the molecule is still not able to dynamically reach distances past 8.5 Å; this is because significant electron density remains between the nuclei, holding the molecule together. This is what is responsible for the weak positive slope in the dynamical energy surface at long distances seen in Figure 2b: even though the molecule would prefer to dissociate at equilibrium, there is no easy kinetic pathway to achieve dissociation following the actual photoexcitation.

In addition to the inability of the excited-state wave function to achieve the correct configuration for dissociation, there is a second reason the dynamical energy surface for the photodissociation of Na_2^+ in liquid THF looks so different: the chemical identity of the molecule changes during photo-

dissociation in a way that cannot be accounted for in the gas phase or at equilibrium. At the Franck−Condon ground-state equilibrium distance, the molecule prefers to reside in the $Na(THF)_4$−$Na(THF)_5^+$ coordination state. As the Na−Na distance is increased at equilibrium on the excited state, Figure 4c shows that the coordination state changes to predominantly $Na(THF)_5$−$Na(THF)_5^+$ by 5.4 Å and to the $Na(THF)_5$−$Na(THF)_6^+$ state by 8.5 Å, the result of the extra space available to form additional dative bonds, which are shown as yellow lines. However, during the photodissociation process, Figure 4d shows that there has been insufficient rearrangement of the coordination complex to allow an additional dative bond to form when the Na−Na distance reaches 5.4 Å, and only a single additional dative bond can form by 8.5 Å instead of the two extra dative bonds seen at equilibrium. The insertion of the last dative bond is what is critical to allowing the molecule to fully dissociate, as this is what weakens the bonding electron's association with the more-coordinated sodium core.

To better visualize how the dynamical energy surface describes the photodissociation of Na_2^+ in THF, Figure 5a
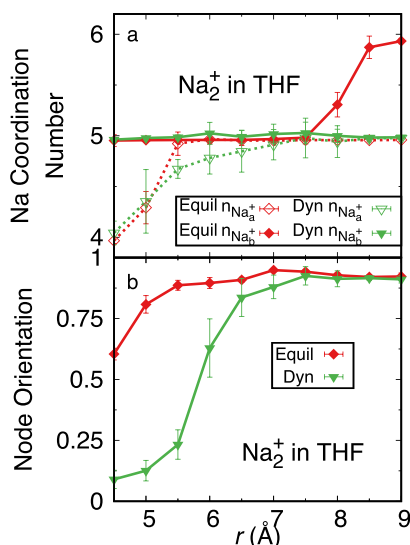

Figure 5. Changes in the $Na_2(THF)_n^+$ chemical identity (i.e., THF coordination number) and the orientation of the bonding electron density explain the dynamical energy surface for the photodissociation of Na_2^+ in THF. Panel a plots the THF dative bond coordination number around each sodium core (more coordinated Na^+, solid curves; less coordinated Na^+, dashed curves) as a function of Na−Na bond length at equilibrium (red) and during the dynamical, nonequilibrium dissociation (green); there is insufficient time for the coordination number to change during the nonequilibrium dynamics to match the equilibrium prediction. Panel b shows the orientation of the excited-state bonding electron's node for at equilibrium (red) and during the dynamical, nonequilibrium dissociation (green) as a function of Na−Na bond length. Clearly, the node rotation is hindered during the nonequilibrium dynamics compared to what happens at equilibrium as a function of Na−Na distance. Together, the inability for the node to rotate and the coordination number to change during dynamics hamper dissociation as reflected in the dynamical energy surface.

plots the number of solvent molecules forming dative bonds with each Na^+ core as a function of the Na−Na bond distance, both at equilibrium on the excited state (red curves) and during the nonequilibrium dynamics (green curves). The dashed curves in this figure show the average number of THF dative bonds to the lesser-coordinated sodium core (referred to as Na_a) while

the solid curves show the number of dative bonds around the more-coordinated sodium core (referred to as Na_b). At equilibrium on the excited state, there are two transitions to new coordination states, a $Na(THF)_4$−$Na(THF)_5^+ \rightarrow Na(THF)_5$−$Na(THF)_5^+$ transition around 5.5 Å and a $Na(THF)_5$−$Na(THF)_5^+ \rightarrow Na(THF)_5$−$Na(THF)_6^+$ transition around 8.5 Å, as visualized in the snapshots in Figure 4c. However, the photodissociation dynamics shows only the first of these transitions (which is not complete until a distance of nearly 7 Å), in concordance with the snapshots shown in Figure 4d.

Figure 5b provides a way to understand how the electronic structure changes at equilibrium and during nonequilibrium dissociation. The plot shows the angle of the node in the excited electronic wave function with respect to the Na−Na bond axis, calculated as an ensemble-averaged dot product of the gas-phase Franck−Condon excited state at the equilibrium ground-state distance with the equilibrium (red diamonds, equilibrated on the excited state) or dynamic (green triangles) excited state at other Na−Na distances. As such, a "node orientation" of zero indicates that the node is perfectly parallel with the Na−Na bond axis while a value of one means that the node is perfectly perpendicular to the Na−Na bond axis. Figure 5b shows that, at equilibrium, the node is able to fully rotate at much lower Na−Na bond distances (∼5.5 Å), whereas, the node does not fully rotate until ∼7 Å in the photodissociation dynamics. Following photoexcitation, the datively bonded THFs do not have time to move to an appropriate position to allow the node to rotate.

The changes in the Na_2^+ chemical identity coupled with the changes in the electronic structure of the bonding electron during the nonequilibrium dissociation of Na_2^+ in THF explain the behavior of the dynamical energy surface shown in Figure 2b. The preliminary "dip" in the dynamical energy surface arises because, upon photoexcitation, the bonding electron's wave function must orient on the fly from a π-like to a σ^*-like electronic structure; in addition, the molecule must potentially change chemical identity through the formation of new Na−THF oxygen-site dative bonds. However, these processes consume the energy the molecule needs to form the final dative bond that at equilibrium takes the loosely bound $Na(THF)_5$−$Na(THF)_5^+$ state to the $Na(THF)_5$−$Na(THF)_6^+$ state allowing the bond to break. This leaves the nonequilibrium molecule without an easy kinetic pathway to dissociate until sufficient time has passed for equilibration to occur.

In summary, through MQC MD simulations of Na_2^+ in the condensed phase, we have shown that nonequilibrium solvent effects are necessary for thinking about photodissociation dynamics and that there are a variety of such effects to consider even for the same solute in different environments. We demonstrated that a dynamical energy surface can be constructed to capture the nonequilibrium solvent effects needed to think about the photodissociation dynamics of Na_2^+ in Ar and in THF. In liquid Ar, the dynamical energy surface directly captures the initial collision of the dissociating molecule with the surrounding cage of Ar atoms. This singular event is reminiscent of the single collision that causes a breakdown of linear response in photofragment rotational dynamics.[42,43] The cage effect is clearly dynamical, as it depends on the magnitude of the solvent's mass: heavier masses amplify the bounce-back of the photofragments upon collision with the solvent cage, while sufficiently light masses lead to better agreement with the PMF because the lighter solvent can equilibrate on the time scale of the dissociation dynamics. In liquid THF, the dynamical energy surface reveals that photoexcitation of Na_2^+ leads to a kinetic

trap that originates from solvent-induced changes in the Na_2^+ molecule's chemical identity and electronic structure. During dynamical, nonequilibrium dissociation, the solute is unable to reorient its bonding electron density from the π-bonding-like state created initially upon photoexcitation to the more σ^*-like state that is needed for dissociation. In addition, there is not sufficient time following photoexcitation for the molecule to undergo the change in chemical identity via the creation of new dative bonds with the solvent, which is also needed for the bond to fully break. All of this work shows that understanding nonequilibrium solvent effects is important for thinking about solution-phase photodissociation dynamics and that an appropriately constructed dynamical energy surface captures a variety of solvent effects that affect the nonequilibrium dynamics in different ways.

Overview of Simulation Details. The work in this paper consists of mixed quantum classical (MQC) molecular dynamics (MD) simulations of Na_2^+ in the condensed phase. In these simulations, which were performed in the microcanonical ensemble, we treated the Na_2^+ molecule as two classical Na^+ cores held together by a single quantum-mechanically treated valence bonding electron plus hundreds of classical solvent molecules. The interactions between the classical particles and the quantum mechanical electron were accounted for using Phillips−Kleinman (PK) pseudopotentials,[44] modified with polarization potentials to correct for the frozen-core approximation implicit in the PK formalism. These pseudopotentials, which are identical to those used in our previous studies,[14−16,33,34,45] are described in more detail in the Supporting Information. The classical interactions between the Na^+ cations and the Ar and rigid OPLS THF solvent molecules were modeled with the same potentials used in our earlier studies in these solvents[14,16] and are detailed in the Supporting Information.

The cubic simulation cells had a side length of 43.8 Å for simulations in Ar and 32.5 Å for those in THF, which given the number of solvent molecules yielded densities of 1.26 g/mL at 120 K for Ar 0.89 g/mL at ∼298 K for THF. In Ar, we expanded the electronic eigenstates of the quantum mechanical electron in a basis of $32 \times 32 \times 32$ plane waves over a 25 $Å^3$ box. Due to the diffuse nature of the valence electron's excited state in THF, particularly at larger Na−Na distances, we used $64 \times 64 \times 64$ plane waves that spanned the entire cubic simulation cell. For all simulations, we utilized periodic boundary conditions with the minimum image convention.[39] All interactions in the cell were tapered smoothly to zero at 16 Å over a 2 Å range using a center-of-mass-based switching function.[46] The single-electron Hamiltonian, which is shown explicitly in the Supporting Information, was diagonalized at every MD time step using the implicitly restarted Lanczos method as implemented in ARPACK.[47] For simulations in THF, the solvent molecules were treated as rigid, planar five-membered rings following the work of Chandrasekar and Jorgensen.[48] All simulations were propagated using the velocity Verlet algorithm[39] with a 4 fs time step, except for simulations with light Ar in which case a 2 fs time step was used.

We performed both equilibrium umbrella sampling, where the Na_2^+ bond length was restrained on either the ground or first excited electronic state, and nonequilibrium dissociation trajectories, where the molecule was placed into the excited state from its equilibrium ground-state configuration and then propagated adiabatically on its electronic excited state. For umbrella sampling in Ar, bins were set at every 0.1 Å from 3.0 Å

out to a dissociative distance of 9.0 Å. For umbrella sampling in THF, bins were set every 0.1 Å from 4.0 Å out to a dissociative distance of 10.0 Å. Within each bin after appropriate equilibration, umbrella trajectories were run for 10 ps to ensure ample statistics across the potential of mean force. Details of the umbrella sampling and the MBAR process used to stitch the individual umbrella sampled windows together to create the PMFs shown in Figure 1 are given in the Supporting Information. For the nonequilibrium trajectories, the Na_2^+ molecule was placed in the first excited state starting from uncorrelated ground-state configurations taken from an equilibrated ground-state trajectory; 15 nonequilibrium trajectories were run in Ar and 20 nonequilibrium trajectories were run in THF to provide statistics for nonequilibrium ensemble averages. Details of the initial configurations chosen for these studies as well as the process used to construct the PMFs and dynamical energy surfaces shown in Figures 1 and 2 are provided in the Supporting Information.

■ ASSOCIATED CONTENT

Ⓢ Supporting Information

The Supporting Information is available free of charge at https://pubs.acs.org/doi/10.1021/acs.jpclett.0c02515.

> Simulation and analysis details, LJ and Coulomb potential parameters, parameters used in the construction of the sodium-electron pseudopotential, functional form and parameters of the fit to the exact e^-THF effective potential, trajectories of the photodissociation and snapshots of excited-state Na_2^+ in Ar, Dynamic potentials of mean force for Na_2^+ in THF (PDF)

■ AUTHOR INFORMATION

Corresponding Authors

Andy Vong − *Department of Chemistry & Biochemistry, University of California, Los Angeles, Los Angeles, California 90095-1569, United States*; Email: andyvong@chem.ucla.edu

Devon R. Widmer − *Department of Chemistry & Biochemistry, University of California, Los Angeles, Los Angeles, California 90095-1569, United States*; Email: widmer@chem.ucla.edu

Benjamin J. Schwartz − *Department of Chemistry & Biochemistry, University of California, Los Angeles, Los Angeles, California 90095-1569, United States;* ⓞ orcid.org/0000-0003-3257-9152; Email: schwartz@chem.ucla.edu

Complete contact information is available at:
https://pubs.acs.org/10.1021/acs.jpclett.0c02515

Author Contributions

#A.V. and D.R.W. contributed equally to this paper.

Notes

The authors declare no competing financial interest.
The computer code used in this study is available from the authors upon reasonable request.

■ ACKNOWLEDGMENTS

ment (XSEDE), which is supported by National Science Foundation grant number ACI-1548562.[49]

■ REFERENCES

(1) Harris, A. L.; Brown, J. K.; Harris, C. B. The nature of simple photodissociation reactions in liquids on ultrafast time scales. *Annu. Rev. Phys. Chem.* **1988**, *39*, 341−356.

(2) Douady, J.; Jacquet, E.; Giglio, E.; Zanuttini, D.; Gervais, B. Non-adiabatic molecular dynamics of excited Na_2^+ solvated in Ar_{17} clusters. *Chem. Phys. Lett.* **2009**, *476*, 163−167.

(3) Niv, M. Y.; Bargheer, M.; Gerber, R. B. Photodissociation and recombination of F_2 molecule in Ar_{54} cluster: Nonadiabatic molecular dynamics simulations. *J. Chem. Phys.* **2000**, *113*, 6660−6672.

(4) Winter, N.; Chorny, I.; Vieceli, J.; Benjamin, I. Molecular dynamics study of the photodissociation and photoisomerization of ICN in water. *J. Chem. Phys.* **2003**, *119*, 2127−2143.

(5) Zanuttini, D.; Douady, J.; Jacquet, E.; Giglio, E.; Gervais, B. Nonadiabatic molecular dynamics of photoexcited Li_2^+ Ne_n clusters. *J. Chem. Phys.* **2011**, *134*, 044308.

(6) Wang, W. N.; Nelson, K. A.; Xiao, L.; Coker, D. F. Molecular-dynamics simulation studies of solvent cage effects on photo-dissociation in condensed phases. *J. Chem. Phys.* **1994**, *101*, 9663−9671.

(7) Peslherbe, G. H.; Ladanyi, B. M.; Hynes, J. T. Trajectory study of photodissociation dynamics in the $NaI(H_2O)$ cluster system. *J. Phys. Chem. A* **1998**, *102*, 4100−4110.

(8) Otto, B.; Schroeder, J.; Troe, J. Photolytic cage effect and atom recombination of iodine in compressed gases and liquids: Experiments and simple models. *J. Chem. Phys.* **1984**, *81*, 202−213.

(9) Parson, R.; Faeder, J.; Delaney, N. Charge flow and solvent dynamics in the photodis- sociation of solvated molecular ions. *J. Phys. Chem. A* **2000**, *104*, 9653−9665.

(10) Schroder, H.; Gabriel, H. Classical simulation of a cage effect in the dissociation of I_2Rg_n clusters (Rg = Ar,Kr,Xe; n=5). *J. Chem. Phys.* **1996**, *104*, 587−598.

(11) Bihary, Z.; Zadoyan, R.; Karavitis, M.; Apkarian, V. A. Dynamics and the breaking of a driven cage: I_2 in solid Ar. *J. Chem. Phys.* **2004**, *120*, 7576−7589.

(12) Liu, Q. L.; Wang, J. K.; Zewail, A. H. Femtosecond dynamics of dissociation and recombination in solvent cages. *Nature* **1993**, *364*, 427−430.

(13) Batista, V. S.; Coker, D. F. Nonadiabatic molecular dynamics simulations of the photofragmentation and geminate recombination dynamics in size-selected I_2^--Arn cluster ions. *J. Chem. Phys.* **1997**, *106*, 7102−7116.

(14) Glover, W. J.; Schwartz, B. J. How does a solvent affect chemical bonds? Mixed quantum/classical simulations with a full CI treatment of the bonding electrons. *J. Phys. Chem. Lett.* **2010**, *1*, 165−169.

(15) Widmer, D. R.; Schwartz, B. J. Solvents can control solute molecular identity. *Nat. Chem.* **2018**, *10*, 910−916.

(16) Widmer, D. R.; Schwartz, B. J. The role of the solvent in the condensed-phase dy- namics and identity of chemical bonds: The case of the sodium dimer cation in THF. *J. Phys. Chem. B* **2020**, *124*, 6603−6616.

(17) Kirkwood, J. G. Statistical Mechanics of Fluid Mixtures. *J. Chem. Phys.* **1935**, *3*, 300−313.

(18) Timko, J.; Castro, A. D.; Kuyucak, S. Ab initio calculation of the potential of mean force for dissociation of aqueous Ca-Cl. *J. Chem. Phys.* **2011**, *134*, 204510.

(19) Zhang, C.; Giberti, F.; Sevgen, E.; de Pablo, J. J.; Gygi, F.; Galli, G. Dissociation of salts in water under pressure. *Nat. Commun.* **2020**, *11*, 3037.

(20) Pham, V.-T.; Fulton, J. L. Ion-pairing in aqueous $CaCl_2$ and RbBr solutions: Simul- taneous structural refinement of XAFS and XRD data. *J. Chem. Phys.* **2013**, *138*, 044201.

(21) Badyal, Y. S.; Barnes, A. C.; Cuello, G. J.; Simonson, J. M. Understanding the effects of concentration on the solvation structure of Ca^{2+} in aqueous solution. II: Insights into longer range order from neutron diffraction isotope substitution. *J. Phys. Chem. A* **2004**, *108*, 11819−11827.

(22) Schmidt, C. Raman spectroscopic determination of carbon speciation and quartz solu- bility in H_2O + Na_2CO_3 and H_2O + $NaHCO_3$ fiuids to 600°C and 1.53 GPa. *Geochim. Cosmochim. Acta* **2014**, *145*, 281−296.

(23) Voth, G. A. Computer simulation of proton solvation and transport in aqueous and biomolecular systems. *Acc. Chem. Res.* **2006**, *39*, 143−150.

(24) King, G.; Warshel, A. Investigation of the free energy functions for electron transfer reactions. *J. Chem. Phys.* **1990**, *93*, 8682−8692.

(25) Hammes-Schiffer, S. Theoretical Perspectives on proton-coupled electron transfer re- actions. *Acc. Chem. Res.* **2001**, *34*, 273−281.

(26) Wong, K. F.; Watney, J. B.; Hammes-Schiffer, S. Analysis of electrostatics and corre- lated motions for hydride transfer in dihydrofolate reductase. *J. Phys. Chem. B* **2004**, *108*, 12231−12241.

(27) Ishida, T.; Hirata, F.; Kato, S. Solvation dynamics of benzonitrile excited state in polar solvents: A time-dependent reference interaction site model self-consistent field approach. *J. Chem. Phys.* **1999**, *110*, 11423−11432.

(28) Ishida, T.; Rossky, P. J. Consequences of strong coupling between solvation and elec- tronic strucure in the excited state of a betaine dye. *J. Phys. Chem. B* **2008**, *112*, 11353−11360.

(29) Koch, D. M.; Timerghazin, Q. K.; Peslherbe, G. H.; Ladanyi, B. M.; Hynes, J. T. Nonadiabatic Trajectory Studies of $NaI(H_2O)_n$ Photodissociation Dynamics. *J. Phys. Chem. A* **2006**, *110*, 1438−1454.

(30) Jarzynski, C. Nonequilibrium Equality for Free Energy Differences. *Phys. Rev. Lett.* **1997**, *78*, 2690−2693.

(31) Kahros, A.; Schwartz, B. J. Going beyond the frozen core approximation: development of coordinate-dependent pseudopoten-tials and application to Na_2^+. *J. Chem. Phys.* **2013**, *139*, 149901.

(32) Szaz, L. *Pseudopotential Theory of Atoms and Molecules*; Wiley: New York, 1985.

(33) Glover, W. J.; Larsen, R. E.; Schwartz, B. J. The roles of electronic exchange and correlation in charge-transfer-to-solvent dynamics: Many-electron non-adiabatic mixed quantum/classical simulations of photoexcited sodium anions in the condensed phase. *J. Chem. Phys.* **2008**, *129*, 164505.

(34) Smallwood, C. J.; Mejia, C. N.; Glover, W. G.; Larsen, R. E.; Schwartz, B. J. A computationally efficient exact pseudopotential method. 2. Application to the molec- ular pseudopotential of an excess electron interacting with tetrahydrofuran (THF). *J. Chem. Phys.* **2006**, *125*, 074103.

(35) Glover, W. J.; Larsen, R. E.; Schwartz, B. J. First principles multi-electron mixed quantum/classical simulations in the condensed phase. II. The charge-transfer-to- solvent states of sodium anions in liquid tetrahydrofuran. *J. Chem. Phys.* **2010**, *132*, 144102.

(36) Glover, W. J.; Larsen, R. E.; Schwartz, B. J. The nature of sodium atoms/$(Na^+$-$e^-)$ contact pairs in liquid tetrahydrofuran. *J. Phys. Chem. B* **2010**, *114*, 11535−115439.

(37) Gervais, B.; Giglio, E.; Jacquet, E.; Ipatov, I.; Reinhard, P. G.; Suraud, E. Simple DFT model of clusters embedded in rare gas matrix: Trapping sites and spectroscopic properties of Na embedded in Ar. *J. Chem. Phys.* **2004**, *121*, 8466−8480.

(38) Glover, W. J.; Larsen, R. E.; Schwartz, B. J. Simulating the formation of sodium:electron tight-contact pairs: Watching the solvation of atoms in liquids one molecule at a time. *J. Phys. Chem. A* **2011**, *115*, 5887−5894.

(39) Allen, M. P.; Tildesley, D. J. *Computer Simulation of Liquids*; Oxford University Press: London, 1992.

(40) Shirts, M. R.; Chodera, J. D. Statistically optimal analysis of samples from multiple equilibrium states. *J. Chem. Phys.* **2008**, *129*, 124105.

(41) Batista, V. S.; Coker, D. F. Nonadiabatic molecular dynamics simulation of ultrafast pump-probe experiments on I_2 in solid rare gases. *J. Chem. Phys.* **1997**, *106*, 6923−6941.

(42) Moskun, A. C.; Jailaubekov, A. E.; Bradforth, S. E.; Tao, G.; Stratt, R. M. Rotational coherence and a sudden breakdown in linear

response seen in room-temperature liq- uids. *Science* **2006**, *311*, 1907−1911.

(43) Tao, G.; Stratt, R. M. The molecular origins of nonlinear response in solute energy relaxation: The example of high-energy rotational relaxation. *J. Chem. Phys.* **2006**, *125*, 114501.

(44) Phillips, J. C.; Kleinman, L. New method for calculating wave functions in crystals and molecules. *Phys. Rev.* **1959**, *116*, 287−294.

(45) Smallwood, C. J.; Larsen, R. E.; Glover, W. G.; Schwartz, B. J. A computationally effi- cient exact pseudopotential method. I. Analytic reformulation of the Philips-Kleinman theory. *J. Chem. Phys.* **2006**, *125*, 074102.

(46) Steinhauser, O. Reaction field simulation of water. *Mol. Phys.* **1982**, *45*, 335−348.

(47) Allen, M. P.; Tildesley, D. J. *ARPACK Users' Guide, Solution of LargeScale Eigen- value Problems with Implicitly Restarted Arnoldi Methods*; SIAM: Philadelphia, 1998.

(48) Chandrasekhar, J.; Jorgensen, W. L. The nature of dilute-solutions of sodium-ion in water, methanol, and tetrahydrofuran. *J. Chem. Phys.* **1982**, *77*, 5080−5089.

(49) Towns, J.; Cockerill, T.; Dahan, M.; Foster, I.; Gaither, K.; Grimshaw, A.; Hazlewood, V.; Lathrop, S.; Lifka, D.; Peterson, G. D.; et al. XSEDE: Accelerating Scientific Discovery. *Comput. Sci. Eng.* **2014**, *16*, 62−74.